Improved Detector Response Characterization Method in ISOCS and LabSOCS

R. Venkataraman[*1], F. Bronson[1], V. Atrashkevich[1], M. Field[1] , and B.M. Young[1].

[1]Canberra Industries, 800 Research Parkway, Meriden, CT 06450, USA

Abstract

The In-Situ Object Calibration Software (ISOCS) and the Laboratory Sourceless Calibration Software (LabSOCS) developed and patented by Canberra Industries have found widespread use in the gamma spectrometry community. Using the ISOCS methodology, one can determine the full energy peak efficiencies of a Germanium detector in the 45 keV – 7 MeV energy range, for practically any source matrix and geometry. The underlying mathematical techniques used in ISOCS (and LabSOCS) have undergone significant improvements and enhancements since their first release in 1996. One of these improvements is a spatial response characterization technique that is capable of handling the large variations in efficiency that occurs within a small region. The technique has been in use in ISOCS and LabSOCS releases since 1999, and has significantly improved the overall quality of the close-in and off-axis response characterization for HPGe detectors, especially for Canberra's Broad Energy Germanium (BEGe) detectors. In this method, the detector response is characterized by creating a set of fine spatial efficiency grids at 15 energies in the 45 keV – 7 MeV range. The spatial grids are created in (r,θ) space about the detector, with the radius r varying from 0 to 500 meters, and the angle θ varying from 0 to π. The reference efficiencies for creating the spatial grids are determined from MCNP calculations using a validated detector model. Once the efficiency grids are created, the detector response can be determined at any arbitrary point within a sphere of 500-meter radius, and at any arbitrary energy within the specified range. Results are presented highlighting the improved performance achieved using the gridding methodology.

Paper presented at the Methods and Applications of Radioanalytical Chemistry (MARC VI) conference, April 7-11, 2003, Kailua-Kona, Hawaii, USA

1. General Philosophy of ISOCS Detector Characterization

The ISOCS detector characterization method uses mathematical techniques to determine gamma ray full energy peak efficiencies of germanium detectors, in vacuum, at an arbitrary energy and spatial location within the characterization range. The response characterization is used with the ISOCS or LabSOCS software package, which factors in the attenuation through any absorbing materials that may be present between the source point and the detector. The general philosophy of ISOCS characterization can be described as follows. A detailed MCNP[1] model of the specific germanium detector is created using the nominal dimensions provided by Canberra's production facility. Dimensions such as the length and diameter of the Ge crystal, the thickness of the dead layer(s), detector well dimensions, holder and endcap dimensions etc. are used in developing the MCNP model. The detector model is validated by comparing MCNP efficiencies to measured efficiencies for several source geometries and at a range of energies. If necessary, minor changes are made to the modeled crystal dimensions and dead layers, and the MCNP efficiencies are re-generated. The detector model is deemed valid if the MCNP efficiencies agree with the measured efficiencies at the 2σ level of uncertainty. Using the validated MCNP model, efficiency data sets are generated, in vacuum, at a large number of point-like locations. Efficiencies are calculated at locations spanning a radial range of 0-500 meters, and at 15 energies in the range between 45 keV to 7 MeV. These efficiency data sets serve as the reference values, which are then meshed together into a single characterization file to be used with the ISOCS or LabSOCS user interface software.

2. Response Characterization Methodologies

2.1 Initial Method

The detector characterization method used in the initial releases of ISOCS (versions 1.x) was based on polynomial fits to MCNP data. About 200 point locations were chosen to

uniformly fill a semi-circular plane extending from 0 degrees (i.e. on the detector axis, in front of the detector) to 180 degrees (i.e. behind the detector), and extending from the center of the front face of the detector endcap out to a radius of 60 meters. The semi-circular region was divided into forward and backward hemispheres, separated by a line parallel to and coinciding with the front face of the detector endcap. The MCNP data points within each hemisphere were then fitted using a set of polynomials that describe the efficiency as a function energy and position in the semicircular plane. The detector is cylindrically symmetric about its axis, and so is the efficiency response. Given the set of polynomial coefficients, the detector response at any location within a radius of 60 meters and at any energy between 50 keV to 7 MeV could be determined.

The polynomial fit based method worked well except for those cases where a large variation in efficiency within a small spatial region had to be modeled. For example, Canberra's BEGe detectors are manufactured with copper holders for lower background. Low energy efficiencies for source locations that are just above the endcap and just below the endcap along the 90º directions can be widely different (2 to 3 orders of magnitude). This was the region where the forward and backward hemispheres met, and the efficiency interpolation between the two sets of polynomials was very difficult. It was necessary to improve the detector characterization method.

A new grid based response characterization method was conceived and implemented in the year 1999. Also, a new measurement protocol was implemented to validate the MCNP model of the detector.

2.2 Validation Measurement Protocol

To validate the detector model, measurements are performed in five different source geometries. A NIST traceable ^{241}Am-^{152}Eu point source and a mixed gamma filter paper standard source are used in the measurements. The point source is counted at a distance of 30 cm away from the center of the front face of the detector endcap, at angular

locations of 0º (on-axis), 90º, and 135º with respect to the symmetry axis of the detector. A specially built source-positioning jig is used to locate the point source at a given angle (Figure 1). The jig consists of a radial arm with a source holder located at the end of the arm. The radial arm can be rotated about a pivotal point and can be fixed at a required angle. Three point source measurements are performed at the 90° angular locations, with the radial arm fixed at azimuthal angles of 120°, 240°, and 360°. These are performed to verify that the Ge crystal is mounted symmetrically inside the endcap. The filter paper is counted by placing it on top of the endcap and then at a distance of 10.16 cm (4 inches) from the endcap. To validate the detector model, the MCNP efficiencies from each of the five source geometries are compared against the corresponding measured efficiencies. The parameters of the MCNP model are adjusted to provide optimum agreement between the model and measured efficiencies.

2.3 Improved characterization method based on gridding techniques

Once the MCNP model of the detector is validated against measured efficiencies, the model is used to generate energy, efficiency, and uncertainty triplets. The triplets are generated at a large number of point source locations, in vacuum, and at 15 energies between 45 keV and 7000 keV. The point source locations are chosen to fill a semicircular plane extending from 0 degrees (i.e. on the detector axis, in front of the detector) to 180 degrees (i.e. behind the detector), and extending from the center of the front face of the detector endcap out to a radius of 500 meters. The point locations are generated in Ln(R)-θ coordinates, R being the radius in millimeters, and θ being the angle in radians (Figure 2). The X-axis represents the angle θ, and the Y-axis represents Ln(R). Characteristic features such as the EndCap (EC) front, the EC side and the EC length have been labeled as such. For purposes of illustration, a profile of the endcap was generated using the function (ECRadius/Sinθ). At θ values very close to 180º, the line representing the endcap profile is not physical and should be disregarded. For the detector profiled in Figure 2, the radius and length of the endcap were 41.25 mm and 133

mm, respectively. As seen from Figure 2, the points are in a grid pattern, spanning the entire semicircular plane. The number of point locations depends on the size of the crystal and the dimensions of the detector endcap. The density of points at the vicinity of the detector endcap is higher than in other regions.

The MCNP calculations described above, yield reference efficiencies at each point source location in the Ln(R)-θ grid, at 15 different energies. The reference data points are distributed in the pattern of a sparse grid. A finer version of the Ln(R) - θ grid is generated as follows. The θ values are represented along the X-axis of the grid, the Ln(R, mm) values are along the Y-axis, and the efficiency values are represented along the Z-axis. All reference (MCNP) data points are first sorted by the X-coordinate so that the data points with the same X values are grouped. Then, the data points within each group [with the constant X] are sorted by the Y-coordinate, thus generating an ordered set. Next, a large number of interstitial spatial locations (approximately 32000) are generated by considering very small increments of X and Y values. These represent the nodal points of the fine grid. The efficiencies at the nodal points are determined by interpolation using a cubic- spline algorithm. The interpolation scheme is as follows. The X-groups are taken one at a time and the Z-values (efficiency) are interpolated along the Y direction (X constant) at all nodes of the grid. At the end of this step in the gridding process, each row of the grid already contains the points needed for interpolation. Then, the grid rows are taken one by one and the Z-values are interpolated along the X directions [Y constant] at all nodes of the grid. The DCG process thus creates a dense grid of efficiency values in Ln(R)-θ space, at each of the 15 photon energies. The response grids at the 15 energies are then compiled into a single file that represents the ISOCS characterization for the given detector. The efficiency at any arbitrary spatial point between the grid nodes is obtained by linear interpolation along the Ln(R) and θ directions. At a given spatial location, the efficiency at any arbitrary energy between 45 keV and 7000 keV is obtained by parabolic interpolation between the energy grids.

Taking advantage of the cylindrical symmetry of the efficiency response, using the DCG grids, one can determine the specific detector's response to a point source in vacuum,

anywhere within a *sphere* of 500 meter radius, centered about the detector, and at any energy between 45 keV and 7 MeV. The ISOCS software can then calculate the efficiency for macroscopic sources by integrating the response over the active volume(s) of a given geometry, taking into account the attenuation through the materials in the geometry.

3. Illustration of ISOCS Characterization Method

A Canberra BEGe 5025 detector was characterized using both the old (polynomial) and the new (grid) methods. The BEGe detector is a planar detector with a surface area of 50 cm^2 and a thickness of 2.5 cm. The results obtained using the old characterization are presented in Tables 1a and 1b for point source geometry in the 90º regions. When the ISOCS efficiencies at 91º (backward hemisphere, just below the endcap) are compared against the measured efficiencies at 90º (Table 1a), a significant disagreement is noted especially at lower energies. This illustrates the large variation in the detector response within a limited spatial region. But, when the ISOCS efficiencies at 89º (forward hemisphere, just above the endcap) are compared against the measured efficiencies at 90º, much better agreement is seen.

Tables 2a, 2b, and 2c present the results obtained using the new (current) grid based characterization for the point source at 0º, 90º, and 135º, respectively. The agreement between MCNP and measured efficiencies is well within the 2σ uncertainty limits. Tables 2d and 2e present the results obtained for the filter paper geometries, using the new characterization method. The ratios of MCNP to measured efficiencies are within the 2σ uncertainty limits.

The detector response characteristics are presented in Figures 3 and 4 as Surfer (©Golden Software Inc.) plots. Figure 3 illustrates the BEGe detector response profiles at gamma ray energies of 45 keV and 60 keV, and Figure 4 shows the profile at 662 keV. Each of these plots displays the iso-efficiency contours at a given energy, as a function of Ln(R) and θ coordinates. In the Surfer plots, the X-axis represents θ, the Y-axis represents

Ln(R), and the Z-axis represents [$-\mathrm{Log}_{10}$(Efficiency)]. Also shown in the plots, is an outline of the detector endcap. In the low energy profiles, the variation in efficiencies in the vicinity of the 90º regions is very evident. This feature is absent in the high energy profiles. Also, at distances far away from the detector, the iso-efficiency contours become almost parallel to each other and with a constant separation, indicating that the efficiency varies according to inverse square of distance.

4. Tests for Grid Quality

A statistical test is performed to check the interpolation quality of the DCG grids. The test involves a bootstrapping method. First, a secondary set of point source locations is generated, intermediate to the primary set of points. The ISOCS efficiencies at the secondary points are determined by linear interpolation, using the primary DCG grids. Using the efficiencies at the intermediate points, a secondary set of DCG grids are created. From the secondary DCG, the efficiencies at the primary point locations are determined, and compared to the MCNP efficiencies at the primary points. Within a specified spatial region, the relative deviation with respect to the MCNP efficiencies is given as follows:

$$\%RD = 100 \bullet \frac{(ISOCSeff - MCNPeff)}{MCNPeff} \qquad (1)$$

The Average Relative Deviation (ARD) is given by,

$$\mathrm{ARD} = \frac{\Sigma \mathrm{RD}}{\mathrm{N}} \qquad (2)$$

where N is the number of points in the specified region.

$$\text{Standard Deviation of RD} = \frac{\sqrt{\Sigma(\mathrm{RD} - \mathrm{ARD})^2}}{\mathrm{N}} \qquad (3)$$

The target value for %ARD is ±1% at all energies, and the target value for the standard deviation is ±2% at all energies.

Contour plots indicating the relative deviation between the primary and secondary DCG grids are provided as a visual aid to determine the interpolation quality. For a given DCG energy, the deviation of the ISOCS efficiencies at the nodes of the secondary DCG grid are determined relative to the efficiencies at the same nodes of the primary DCG grid. The relative deviation values are plotted as contour maps using the Surfer software, in the Ln(R) and θ coordinates. Figure 5 is an example of such a plot. Relative deviation values equal to or above $\pm$ 2% are shown as closed contours in the spatial regions where they occur. A visual inspection of these plots helps users to know the quality of the detector response characterization, in any spatial region where they may locate sources.

5. Conclusions

The new (current) grid based method is very robust and can handle large variations in efficiencies within small spatial regions. The method has significantly improved the accuracy of BEGe detector characterizations. The maximum range of ISOCS characterizations has been extended to 500 meters.

6. References

[1] Breismeister, J.F. (ed.), MCNP-A general Monte Carlo N particle Transport Code Version 4B, Los Alamos National Laboratory Report LA-12625-M (March 1997).

Table 1a. Point Source at 90 degrees: ISOCS (91deg) Vs Measured Efficiencies

Source located at 90 degrees		Measured Efficiency		ISOCS Efficiency (91 deg)		Ratio of ISOCS Eff over Measured Eff	
Nuclide	E (keV)	Efficiency	Rel Unc (1σ)	Efficiency	Rel Unc (1σ)	Ratio	Rel Unc (1σ)
AM-241	59.54	1.49E-05	3.78%	8.68E-05	20.00%	5.84	20.35%
EU-152	121.78	6.76E-05	3.62%	1.16E-04	15.00%	1.71	15.43%
	344.27	5.00E-05	3.59%	6.08E-05	13.00%	1.22	13.49%
	778.89	2.75E-05	3.80%	2.72E-05	11.00%	0.99	11.64%
	1112.02	2.12E-05	4.00%	1.97E-05	8.00%	0.93	8.94%
	1407.95	1.83E-05	3.63%	1.62E-05	7.00%	0.88	7.88%
				Weighted Average		0.97	4.70%

Table 1b. Point Source at 90 degrees: ISOCS (89deg) Vs Measured Efficiencies

Source located at 90 degrees		Measured Efficiency		ISOCS Efficiency (89 deg)		Ratio of ISOCS Eff over Measured Eff	
Nuclide	E (keV)	Efficiency	Rel Unc (1σ)	Efficiency	Rel Unc (1σ)	Ratio	Rel Unc (1σ)
AM-241	59.54	1.49E-05	3.78%	1.53E-05	20.00%	1.03	20.35%
EU-152	121.78	6.76E-05	3.62%	7.19E-05	15.00%	1.06	15.43%
	344.27	5.00E-05	3.59%	5.50E-05	13.00%	1.10	13.49%
	778.89	2.75E-05	3.80%	2.86E-05	11.00%	1.04	11.64%
	1112.02	2.12E-05	4.00%	2.30E-05	8.00%	1.08	8.94%
	1407.95	1.83E-05	3.63%	2.00E-05	7.00%	1.09	7.88%
				Weighted Average		1.08	4.56%

Table 2a. Point source On-Axis: Comparison of ISOCS vs Measured Efficiencies

Source located at 0 degree		Measured Efficiency		ISOCS Efficiency		Ratio of ISOCS eff. over Measured eff.	
Nuclide	E (keV)	Efficiency	Rel Unc (1σ)	Efficiency	Rel Unc (1σ)	Ratio	Unc (1σ)
AM-241	59.54	3.63E-03	3.58%	3.59E-03	10.00%	0.990	0.105
Eu-152	121.78	3.29E-03	3.31%	3.30E-03	10.00%	1.003	0.106
	244.6	1.79E-03	3.33%	1.84E-03	8.00%	1.030	0.089
	344.27	1.24E-03	3.31%	1.26E-03	8.00%	1.013	0.088
	778.89	5.19E-04	3.35%	5.20E-04	6.00%	1.001	0.069
	1112.02	3.72E-04	3.39%	3.71E-04	4.00%	0.997	0.052
	1407.95	2.89E-04	3.35%	2.91E-04	4.00%	1.008	0.053
				Weighted Average		1.003	0.028

Table 2b. Point source at 90 deg: Comparison of ISOCS vs Measured Efficiencies

Source located at 90 degrees		Measured Efficiency		ISOCS Efficiency		Ratio of ISOCS eff. over Measured eff.	
Nuclide	E (keV)	Efficiency	Rel Unc (1σ)	Efficiency	Rel Unc (1σ)	Ratio	Unc (1σ)
AM-241	59.54	9.28E-05	3.61%	9.19E-05	10.00%	0.991	0.105
EU-152	121.78	6.48E-04	3.44%	6.56E-04	10.00%	1.012	0.107
	244.6	6.21E-04	3.49%	6.26E-04	8.00%	1.009	0.088
	344.27	5.02E-04	3.44%	5.00E-04	8.00%	0.995	0.087
	778.89	2.73E-04	3.47%	2.80E-04	6.00%	1.026	0.071
	1112.02	2.17E-04	3.48%	2.18E-04	4.00%	1.006	0.053
	1407.95	1.85E-04	3.46%	1.88E-04	4.00%	1.014	0.054
				Weighted Average		1.010	0.029

Table 2c. Point source at 135 deg: Comparison of ISOCS vs Measured Efficiencies

Source located at 135 degrees		Measured Efficiency		ISOCS Efficiency		Ratio of ISOCS eff. over Measured eff.	
Nuclide	E (keV)	Efficiency	Rel Unc (1σ)	Efficiency	Rel Unc (1σ)	Ratio	Unc (1σ)
AM-241	59.54	3.85E-05	4.73%	4.00E-05	10.00%	1.039	0.115
EU-152	121.78	9.85E-04	3.32%	9.79E-04	10.00%	0.993	0.105
	244.6	9.20E-04	3.37%	9.59E-04	8.00%	1.042	0.090
	344.27	7.22E-04	3.31%	7.35E-04	8.00%	1.018	0.088
	778.89	3.58E-04	3.41%	3.63E-04	6.00%	1.013	0.070
	1112.02	2.72E-04	3.42%	2.66E-04	4.00%	0.979	0.052
	1407.95	2.23E-04	3.35%	2.25E-04	4.00%	1.007	0.053
				Weighted Average		1.002	0.028

Table 2d. Glass Fiber Filter Paper on Endcap: ISOCS vs Measured Efficiencies

Energy	Measured Efficiency		ISOCS Efficiency		ISOCS Eff / Meas. Eff	
(keV)	Efficiency	Rel Unc (1σ)	Efficiency	Rel Unc (1σ)	Ratio	Unc (1σ)
59.5	2.56E-01	4.49%	2.74E-01	10.00%	1.070	0.117
88	2.55E-01	4.90%	2.70E-01	10.00%	1.057	0.118
122	2.35E-01	4.20%	2.50E-01	10.00%	1.062	0.115
392	8.51E-02	3.91%	8.85E-02	8.00%	1.040	0.093
662	5.00E-02	4.42%	5.16E-02	6.00%	1.031	0.077
835	3.93E-02	3.99%	4.09E-02	6.00%	1.039	0.075
1115	3.00E-02	4.00%	3.10E-02	4.00%	1.035	0.059
			Weighted Average		1.042	0.032

Table 2e. Glass Fiber Filter Paper 10.17 cm from Endcap: ISOCS vs Measured Efficiencies

Energy	Measured Efficiency		ISOCS Efficiency		ISOCS Eff / Meas. Eff	
(keV)	Efficiency	Rel Unc (1σ)	Efficiency	Rel Unc (1σ)	Ratio	Unc (1σ)
59.5	2.13E-02	4.51%	1.97E-02	10.00%	0.925	0.101
88	2.13E-02	4.93%	1.93E-02	10.00%	0.906	0.101
122	1.98E-02	4.31%	1.79E-02	10.00%	0.905	0.099
392	6.47E-03	3.99%	6.06E-03	8.00%	0.937	0.084
662	3.70E-03	4.51%	3.37E-03	6.00%	0.912	0.068
835	2.90E-03	4.03%	2.77E-03	6.00%	0.954	0.069
1115	2.22E-03	4.04%	2.11E-03	4.00%	0.952	0.054
			Weighted Average		0.933	0.029

Figure 1. Jig to perform point source validation measurements

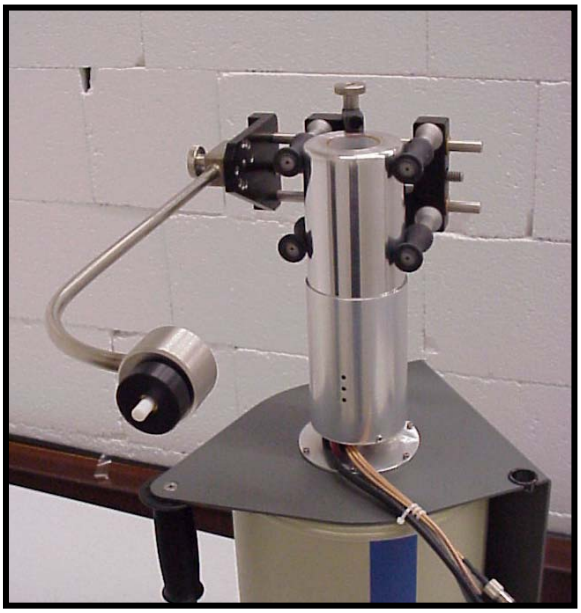

Figure 2. MCNP Point Locations for ISOCS Characterization

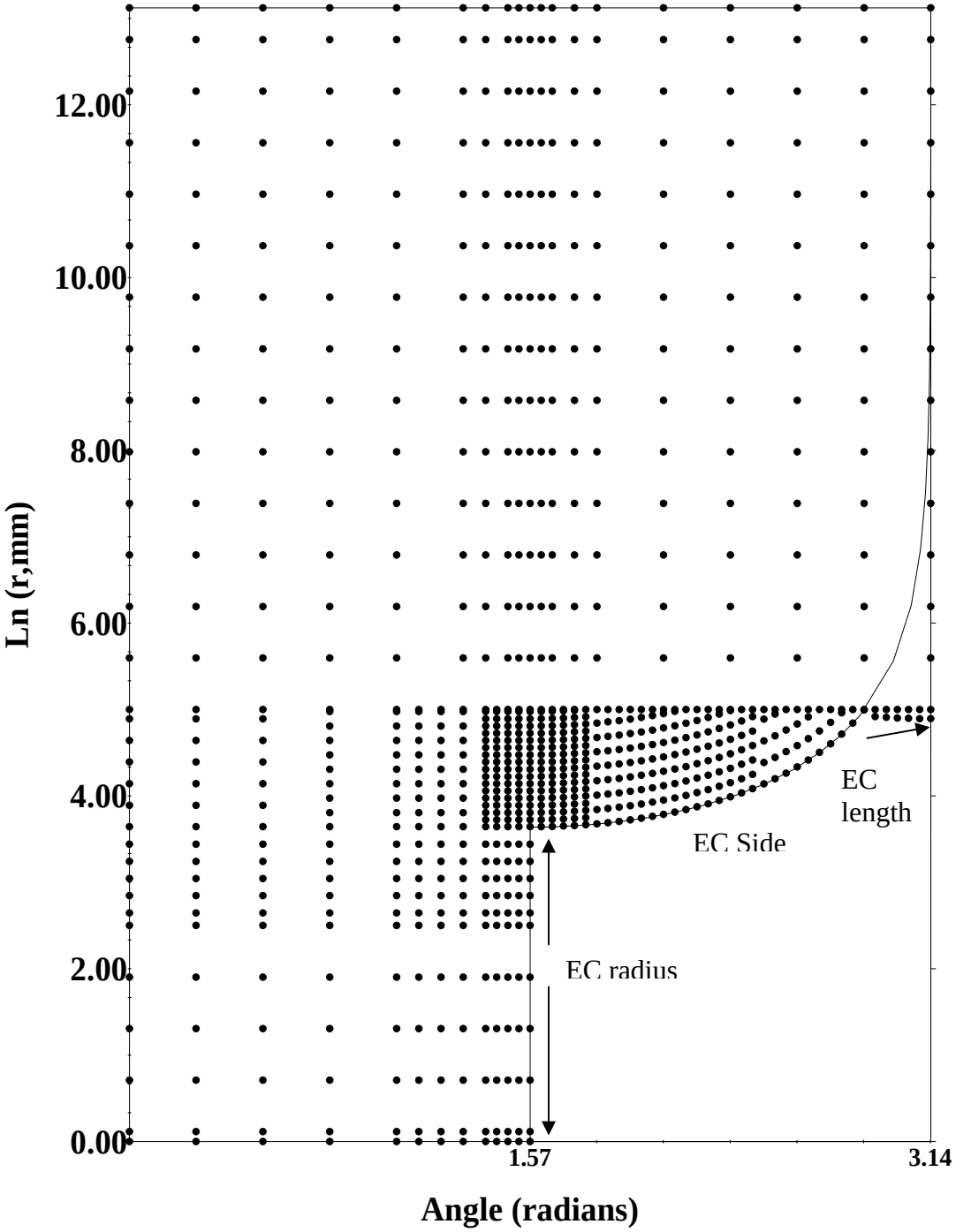

Figure 3. Detector Response Profiles at 45 keV and 60 keV

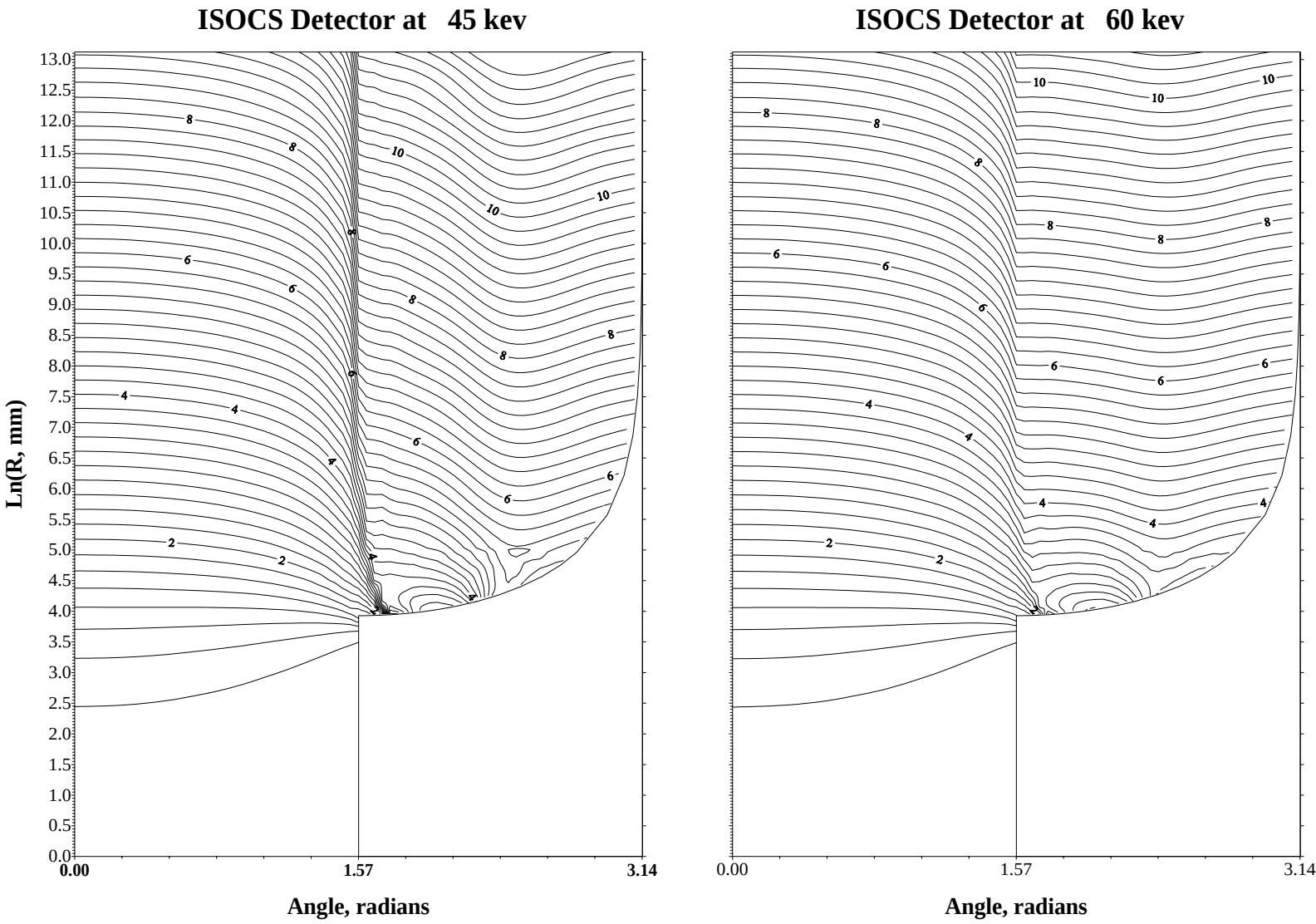

Figure 4. ISOCS Detector at 662 kev

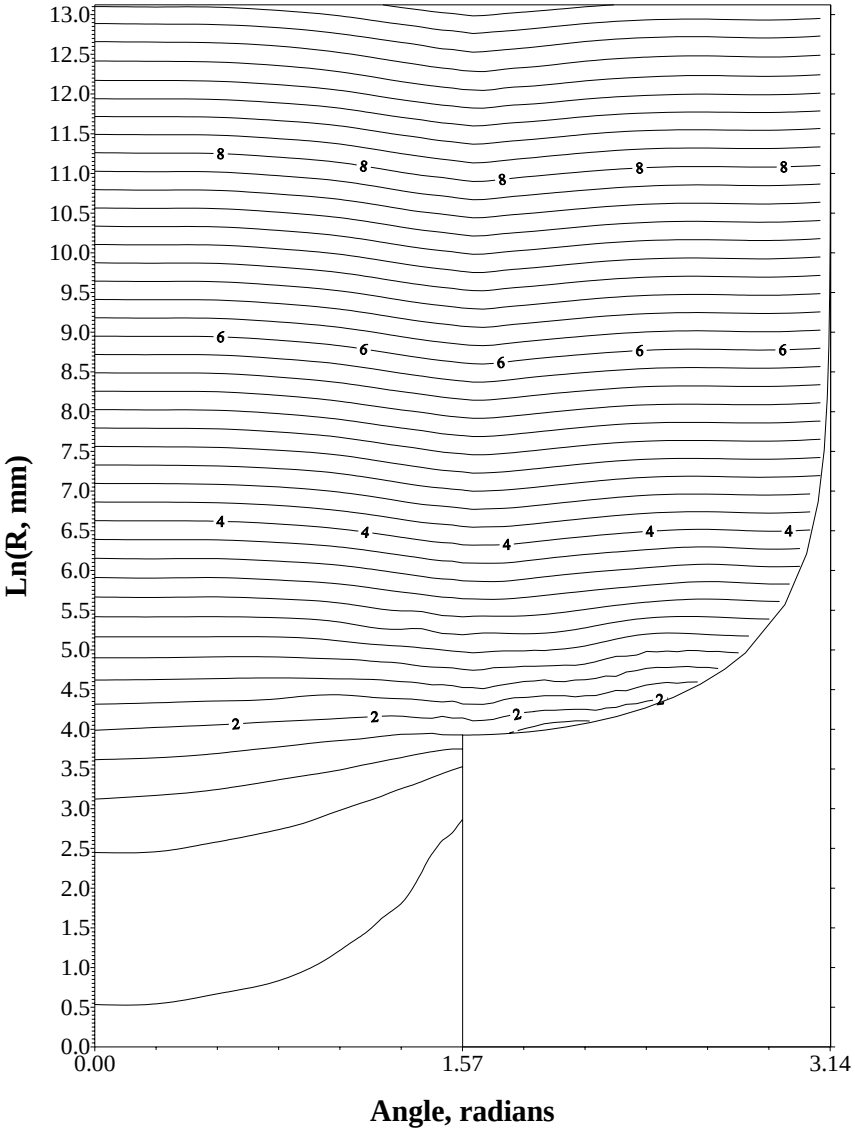

Figure 5. Relative Deviation at 45 kev